Silica seed particles improve the efficiency and throughput of nanoparticle acoustic trapping

Megan Havers,[1,*] Thierry Baasch,[1,†] Andreas Lenshof,[1,‡] Mikael Evander,[2,§] and Thomas Laurell[1,‖]

[1] *Biomedical Engineering Department, Lund University, Ole Römers väg 3, 221 00, Lund, Sweden*
[2] *AcouSort AB, Scheelevägen 14, Lund, 223 63, Sweden*

(Received 12 December 2023; revised 9 February 2024; accepted 9 February 2024; published 11 March 2024)

Silica has rarely been used as a seed particle material in acoustic trapping of nanoparticles. Here we use fluorescent nanoparticles, which are frequently used as a model system, to demonstrate that throughput and nanoparticle trapping efficiency can be improved by using silica seed particles as opposed to traditionally used polystyrene seed particles. The 10 times larger dipole scattering coefficient of silica seed particles compared with polystyrene seed particles in water leads to a higher retention force against fluid flow and thus enables higher throughput. Seed particles retained at an actuation voltage of approximately 10 V p.p. can withstand flow rates up to 2100 ± 200 µl/min for silica and 200 ± 50 µl/min for polystyrene. Furthermore, silica is found to be 40%–2000% more efficient (number of trapped nanoparticles as measured by fluorescent intensity) than polystyrene seed particles in trapping 270-nm polystyrene nanoparticles from suspensions of 10^{10}–10^{11} particles/ml. Moreover, after enriching nanoparticles into a silica seed particle cluster, the washing flow rate can be increased from 30 µl/min to 200 µl/min (the flow rate at which polystyrene clusters are unstable), halving the total sample processing time without losing the silica seed particle cluster or compromising the nanoparticle trapping efficiency. Thus, material properties (particularly density) of the seed particles are critical to both nanoparticle trapping efficiency and throughput.

DOI: 10.1103/PhysRevApplied.21.034016

I. INTRODUCTION

A major obstacle in disease prognosis in medicine is that submicron targets, such as extracellular vesicles carrying biomarkers in biofluids [1–3], are very difficult to isolate in a reliable way [4–7]. In the last decade, acoustic trapping has emerged as a novel technique for nanoparticle (NP) enrichment in fluids [8]. Acoustically enriched extracellular vesicles have provided diagnostic and prognostic information such as surface markers [9,10], microRNAs (small ribonucleic acid molecules) [9], and protein expression [11,12]. Acoustic trapping functions as a fluidic platform able to retain particles and cells against flow in an ultrasonic standing wave field [13,14]. Compared with ultracentrifugation, acoustic trapping is rapid and gentle [9]. Acoustic trapping also allows washing, removing nontrapped species like free proteins [11].

The acoustic forces acting on a particle in an acoustic field depend on the particle's compressibility and density relative to its surroundings, in addition to the particle's volume [15]. The compressibility and density of particles determine the monopole and dipole scattering coefficients, respectively, of the particles in a fluid [16]. Particles that are denser than their surrounding fluid and have a positive acoustic contrast factor (as defined in Ref. [17]) may be retained by acoustic trapping as shown in Fig. 1(a). Fornell *et al.* [18] demonstrated that a particle density contrast to the surrounding fluid is critical to whether acoustic forces retain microparticles against flow. Polystyrene ($\rho = 1050$ kg m^{-3}) and melamine particles ($\rho = 1500$ kg m^{-3}) with 10-µm diameters could both be retained against flow in water, but in a denser fluid (14% Ficoll, $\rho = 1050$ kg m^{-3}) only melamine particles were retained against flow.

Acoustic radiation forces are highly particle-size dependent, which makes trapping of individual submicron particles against fluid flow challenging. In 2012, Hammarström *et al.* [8] observed that 400-nm polystyrene NPs could only

*megan.havers@bme.lth.se
†thierry.baasch@bme.lth.se
‡andreas.lenshof@bme.lth.se
§mikael.evander@acousort.com
‖thomas.laurell@bme.lth.se

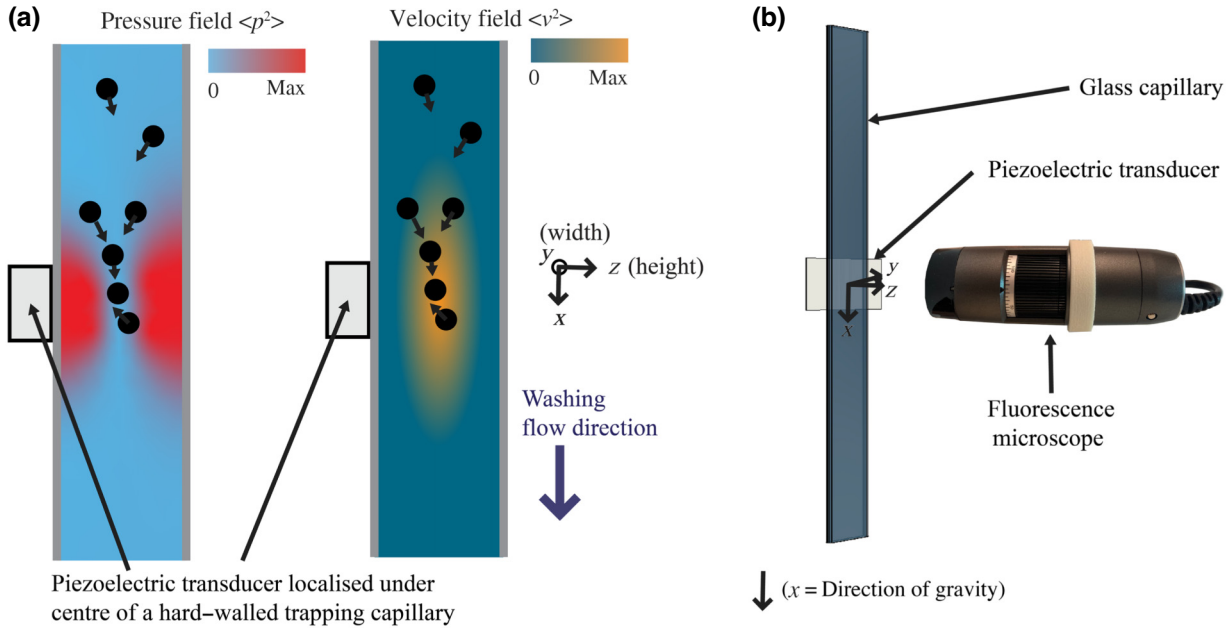

FIG. 1. (a) Schematic of the mean squared pressure (left) and velocity (right) fields generated in a rigid fluid-filled capillary driven at its resonance frequency by a localized piezoelectric transducer. Positive acoustic contrast microparticles are represented by black circles. The pressure and velocity gradients in the z direction above the transducer lead to axial acoustic radiation forces on particles, focusing them to the midheight of the channel. The velocity gradient in the x direction leads to lateral acoustic radiation forces that may retain particles against flow. (b) The experimental setup for particle trapping. The glass capillary dimensions are 2-mm width (y), 0.2-mm height (z), and 40-mm length (x). The trapping region is recorded by a fluorescence microscope, perpendicular to the piezoelectric transducer. Gravity acts in the positive x direction.

be enriched in an acoustic trap when the concentration exceeded 1 wt % (approximately 4×10^{12} particles/ml), hypothesizing that the interparticle distance was short enough for scattered sound interaction between the NPs to induce interparticle forces sufficiently large for NP aggregation. However, using sound-scattering polystyrene seed particles enabled bacteria trapping at concentrations much lower than 1 wt % [8], approaching clinically relevant concentrations of bacteria (1.1×10^5 bacteria/ml). Additionally, trapping 100-nm polystyrene NPs was demonstrated at 0.1 wt % with seed particles, whereas direct capture was not possible even at 1 wt % [8]. Henceforth, in the topical field of acoustofluidics-based extracellular vesicle trapping, it has become standard practice to investigate NP acoustic trapping performance first using polystyrene NPs [9,11,19].

This method of NP acoustic trapping (see Fig. 2) enriches the submicron particles in the interstitial space of the preloaded seed particles (10-μm-diameter polystyrene beads) [8]. The acoustic trapping seed structure concept is similar to earlier work by Gupta and Feke [20], where a chamber packed with glass beads (3 mm in size) was actuated with an acoustic standing wave to retain 2–15-μm polystyrene against flow. In 2014, Silva and Bruus [21] derived the acoustic interaction force on one elastic particle caused by waves scattered from microparticles for any separation distance: the resulting force depends on the inverse interparticle distance to the fourth power. In the case of acoustic trapping, when particles are close to the pressure node, this acoustic interaction force depends on the dipole scattering coefficients and sizes of all the particles involved [22]. The theory for acoustic interparticle forces has been validated experimentally for micrometer-sized particles [22–25].

The trapping of NPs is a complex phenomenon; scattered sound interaction, hydrodynamics and electrostatic forces influence whether NPs can be trapped, although the relative force contributions are unknown. In recent years, theoretical investigations have been made to elucidate some of the effects in acoustic trapping of NPs [26–29]; however, these underlying theories have not yet been experimentally validated with NPs.

Acoustic streaming has also been observed, introducing drag forces that cause nontrapped particles to circulate in the vicinity of the trapping region [8]. The streaming observed in an unloaded trap, without a seed particle cluster present, is considered to be largely induced by thermoviscous effects due to the thermal gradient above the transducer and, to a lesser extent, boundary-driven streaming [30]. With dilute NPs, Hammarström *et al.* [8] observed that the motion of submicron particles, without a seed particle cluster present, was dominated by the

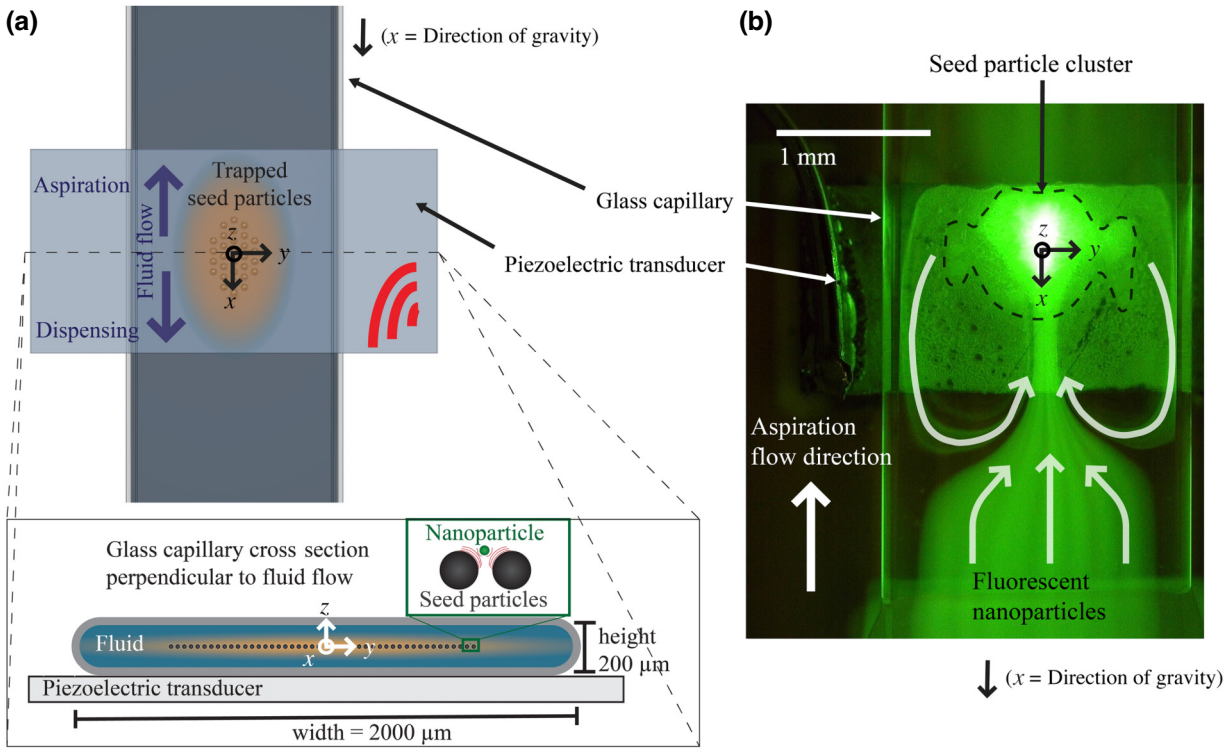

FIG. 2. (a) The acoustic field is represented by the local $\langle v^2 \rangle$ maximum (orange shading) in the center of the capillary cross section. The velocity gradient traps seed particles (10 µm, dark spheres) which scatter sound, between which NPs (<300 nm, green sphere) are trapped. (b) Image of trapping region during aspiration of high concentration NPs (around 10^{12} particles/ml) into the seed particle cluster (step 3 in Fig. 3). Gravity acts in the positive x direction.

streaming rolls, such that the particles could evade trapping. However, it is still unknown to what degree this phenomenon aids or hinders NP trapping when seed particles are present.

Until now, most submicron particle acoustic trapping studies have used preloaded seed particles made of polystyrene [9–12,19,31–37]. An exception was the use of silica seed particles while trapping bacteria for mass spectrometry in 2014 by Hammarström *et al.* [38]. In that case, the choice of material was motivated by the hydrophilic surface properties of silica beads, as it was anticipated that silica seed particles would have less nonspecific binding of proteins than polystyrene seed particles. However, they did not compare bacteria trapping performance of silica seed particles with that of polystyrene seed particles.

In this paper, we investigate the impact of the seed particle material on acoustic trapping efficiency and throughput, where trapping efficiency denotes the number of NPs trapped as measured by fluorescence intensity. We choose to compare silica and polystyrene since both particle types are widely used in bioanalytical assays. Firstly, we aspirate seed particles made of silica or polystyrene into the acoustic field and retain the particle clusters against increasing flow rates. We present quantitative results that demonstrate that silica seed particles display around 10 times greater retention forces and potential for higher throughput trapping as compared with polystyrene seed particles. To our knowledge, this is the first published work showing good agreement between analytical calculations of dipole scattering coefficient with a retention coefficient calculated from experiments in an acoustic trapping capillary. Ley and Bruus [39] previously described a method to measure the acoustic energy density in an acoustic capillary, like the one we use in this study, by increasing flow rate on a test particle until the maximum lateral retention force cannot balance the Stokes drag force any longer. We show that a similar method (see Sec. III E) can be used to determine that the lateral retention force on a seed particle scales as expected with its density.

Secondly, we apply these seed particles for NP trapping. Fluorescence intensity has previously been used to track the trapping of *Escherichia coli* into a polystyrene seed particle cluster, since the fluorescence scales with the number of particles [8]. Here, we measure the fluorescence intensity over time [Fig. 2(b)] to quantify the trapping and washing of fluorescent NPs using silica and polystyrene seed particles. Silica seed particles demonstrate higher NP trapping efficiency and enable greater throughput than polystyrene seed particles. This finding has noteworthy consequences for NP trapping applications and suggests

that more attention should be given to the seed particle material choice to increase throughput and trapping efficiency of NPs in 10^{10}–10^{11} particles/ml suspensions. Both of these are major challenges for isolating extracellular vesicles from biofluids for clinical applications.

II. ACOUSTIC TRAPPING THEORY

Polystyrene and silica are more dense and less compressible than water, see Table I. Thus, microparticles made of silica or polystyrene suspended in water at room temperature have a positive acoustic contrast factor (as defined in Ref. [17]). In zero flow, but in the presence of an acoustic field, these particles will move towards the region where pressure fluctuations are minimum and velocity fluctuations are maximum, see Fig. 1(a).

In acoustic trapping, Fig. 1, a localized acoustic field generated by bulk acoustic waves can be used to suspend particles in a capillary above a piezoelectric transducer. When the actuation frequency matches the half-wavelength resonance of the water-filled capillary, positive acoustic contrast particles in the capillary are focused to the pressure node at the half-height defined as $z = 0$ [see Figs. 1(a) and 2(a)]. The seed particle cluster may be retained at this point against the drag force induced during washing in the x direction when there is a local strong Gor'kov minimum [16,18,39], due to the velocity gradient, Fig. 1(a).

The retention force F_r for a single particle of volume V at point (x, z) in the capillary, with pressure amplitude P_0, angular frequency ω, and wave numbers k_x, k_z, was derived by Fornell *et al.* [18]. Noting the orientation of the device is now defined as in Fig. 1, Eq. (16) in Ref. [18] can be written as

$$F_r = -V\frac{3\,f_2 P_0^2}{8\,\omega^2\rho_f}k_x k_z^2\sin(2k_x x). \tag{1}$$

The dipole scattering coefficient f_2 is defined as

$$f_2 = 2\frac{(\rho_p/\rho_f) - 1}{2(\rho_p/\rho_f) + 1} = 2\frac{\tilde{\rho} - 1}{2\tilde{\rho} + 1}, \tag{2}$$

where ρ_p is the density of the seed particle, ρ_f is the density of the surrounding fluid (997 kg m^{-3} for water at room temperature and pressure), and $\tilde{\rho}$ is the density contrast ρ_p/ρ_f. ω is the angular frequency $(2\pi f)$ of the applied ultrasound. In the device used in this study, the resonance frequency f of the water-filled capillary is 4.1 MHz. For 10-μm seed particles in this acoustic field $ka = \omega a/c = 0.086$, where a is the radius of the seed particle (5×10^{-6} m) and c is the speed of sound in the surrounding fluid (1500 m s^{-1}), thus $ka \ll 1$.

TABLE I. Physical property parameters for seed particles, nanoparticles, and fluid.

Particle	Material	Density[a] (kg m^{-3})	Compressibility[b] ($\times 10^{-10}$ Pa^{-1})	Diameter[a] (μm)	Supplier (lot number)
Fluorescent polystyrene seed particle	Polystyrene	1055	2.45	10.0 ± 0.1	Microparticles GmbH, Germany (PS-FluoGreen-Fi347)
Fluorescent silica seed particle	Silica	1800	0.27	10 ± 2	Kisker Biotech GmbH & Co. KG, Germany (GK072842-09)
Nonfluorescent polystyrene seed particle	Polystyrene	1055	2.45	10.0 ± 0.1	Sigma Aldrich, Germany (BCBN8192V)
Nonfluorescent silica seed particle	Silica	1800	0.27	10 ± 2	Kisker Biotech GmbH & Co. KG, Germany (GK1060743-01)
Fluorescent nanoparticles (NPs)	Polystyrene + Fluoro-Max dye	1055	2.45	0.277 ± 0.050[d]	Thermo Fisher Scientific, US (246584)
Fluid	MilliQ Water	997[c]	4.55		Merck KGaA, Germany (N/A)

[a]From supplier. Unless otherwise stated, particles are smooth and spherical.
[b]Value at 25 °C, from Qiu *et al.* [40]
[c]Values as measured by Han *et al.* [41]
[d]Measured by nanoparticle tracking analysis, see Sec. III D.

The wave numbers in the x and z directions are given by

$$k_x = \frac{2\,\pi}{\lambda_x} = \frac{2\,\pi}{2\,l} \text{ and } k_z = \frac{2\,\pi}{\lambda_z} = \frac{2\,\pi}{2\,h}, \tag{3}$$

where the piezoelectric transducer length l is approximately 2000 μm and $h = 200$ μm is the height of the capillary (Figs. 1 and 2). λ is the corresponding wavelength for each wave number k in the x and z directions.

It is relevant to note that the transducer and capillary length are orientated vertically; this means that, in the absence of both an acoustic field and fluid flow, microparticles with higher density than the fluid will sediment down the length of the capillary. This is in contrast to work by Fornell *et al.* [18], who used a similar device with the capillary laid horizontally, such that the microparticles settled on the bottom wall when the acoustic field was turned off.

According to Eq. (1), the retention force that a particle experiences in an acoustic field depends on its density relative to the fluid. In order to achieve high throughput in NP trapping, see Fig. 2, the seed particle cluster needs to be stable under (or withstand) the effect of the strong drag forces during washing [see Appendix A, Eqs. (A1)–(A5)]. This requires a strong retention force, which is enabled by a large density contrast, Eqs. (1) and (2). The seed particles are particularly useful if they can be retained at a wide range of voltages and flow rates.

The retention force, Eq. (1), was derived for a single isolated particle. The total acoustic radiation force on a cluster of seed particles will be the sum of the primary acoustic radiation force over all particles, while the acoustic particle-particle interactions are approximately equal and opposite for neighboring particles and their contribution to the total retention force cancels over the whole cluster. As the acoustic particle-particle interactions decay quickly with the particle-particle distance [22], we neglect any contributions from non-neighboring particles.

III. MATERIALS AND METHODS

A. Acoustic trapping instrumentation

The AcouTrap (AcouSort AB, Lund, Sweden) system we use possesses a trapping unit consisting of a glass capillary mounted on a piezoelectric transducer [Fig. 1(b)]. Figure 2(a) illustrates the trapping capillary from the field of view, as well as a cross section of the capillary above the piezoelectric transducer.

The ultrasound transducer is actuated with a peak-to-peak voltage of 10 V p.p. (or as otherwise stated), centered at 4.1 MHz, and a frequency tracking system is used to automatically adjust and record the resonance frequency as previously described [42]. When the frequency tracking is active, a resonance frequency scan ±1% around the center frequency is repeated every 1 s to find the frequency of the maximum power input. This tracking accounts for the resonance frequency change with varying temperature (see Appendix B, Fig. 8) or sample composition [42]. Hammarström *et al.* implemented this technique and found for their system that drifting only 50 kHz off resonance decreased the maximum washing flow rate by a factor of 10 [42]. Loading particles in the trap will also change the resonance frequency (see Appendix B, Fig. 9) and going from zero flow to wash flow will alter the fluid temperature in the trap and hence the resonance frequency (Fig. 8). To trap a stable cluster of seed particles and retain them during washing, frequency tracking is a prerequisite to ensure that the seed particle clusters are not lost. Thus, frequency tracking provides a more robust device [42] and is common practice in levitated seed particle acoustic trapping.

During the short time when the frequency scan is performed, the frequency is shifted off resonance by 1%, and this is found to be enough to lose the cluster, especially when changing from zero to very high flow rates. Owing to this, during the seed particle retention quantification experiments, the frequency tracking is deactivated for high-flow-rate ramping steps such that the frequency is fixed to the optimal resonance frequency recorded during the 150-μl/min wash.

The AcouTrap software allows control of the x, y, z position of the capillary, valves, syringe pump flow rate, and magnetic stirring of a vial with seed particles. The magnetic stirring is automated to mix the seed particles for 60 s immediately before aspiration, ensuring consistent seed particle concentrations throughout the experiment. One syringe contains MilliQ water (see Table I for properties and supplier) for dispensing through the capillary. A second, empty, syringe is used to aspirate from the vial or 96-well plate (containing NPs and water).

B. Microscope

A universal serial bus fluorescence microscope AM4115T-GFBW (Dino-Lite Europe) is mounted horizontally, as shown in Fig. 1(b), and focused on the center of the capillary in the region above the transducer. A series of images [such as Fig. 2(b)] are taken whilst illuminating with the light-emitting diode $\lambda_{ex} \sim 488$ nm, with the emission filter $\lambda_{em} \sim 510$ nm. In each experiment, images are taken at 1 s intervals, with an exposure time of 1/1000 s to 1/30 s depending on the fluorescent particle type and concentration to maximize the signal whilst avoiding saturation of the camera pixels. Each image series are exported as a single .wmv video from which the average green pixel intensity is calculated for each frame.

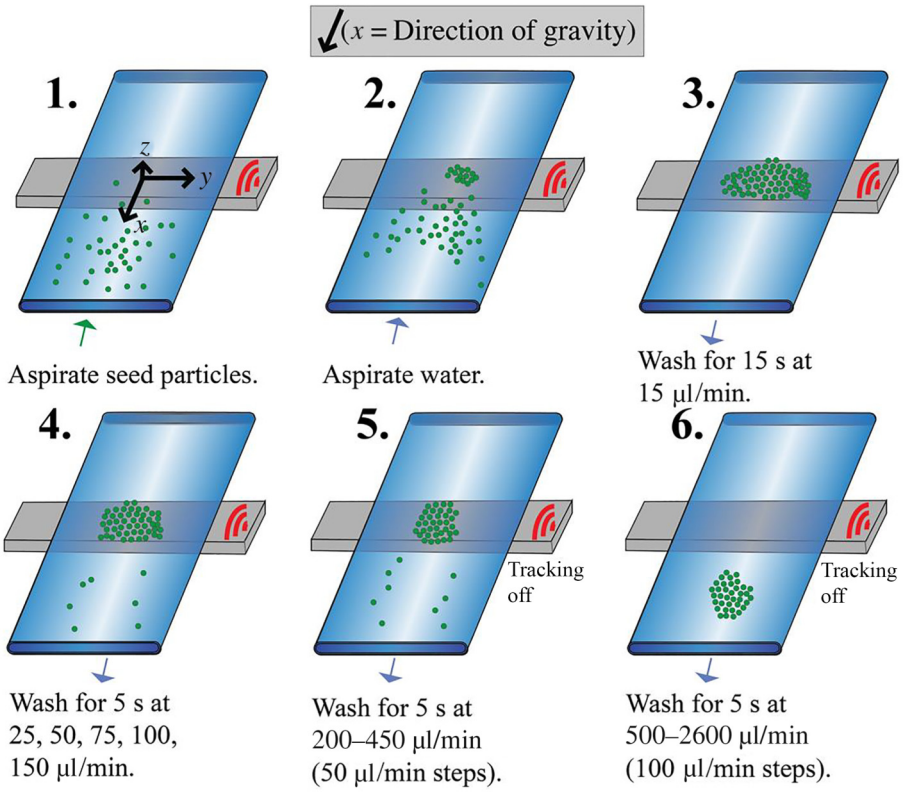

FIG. 3. Schematic of a seed particle cluster washing experiment in an acoustic trapping capillary. The green circles represent fluorescent seed particles. In step 1, freshly stirred seed particles are aspirated at 100 µl/min. Then in step 2, 25 µl of water is aspirated at 75 µl/min to bring the remaining particles up to the transducer region, where they are retained by the acoustic field. Step 3 washes off excess particles with water at 15 µl/min for 15 s. In steps 4 to 6, the flow is ramped up in steps without returning to zero flow. The ultrasound is on for the duration of the experiment; however, tracking is turned off for the higher flow rates (steps 5 to 6). At some point during the ramping, the flow rate becomes too great for the cluster to be retained in the acoustic field, and the cluster is washed away. Gravity acts in the positive x direction.

C. Seed particles

10-µm-sized spherical particles made of either polystyrene or silica are used as seed particles in all studies. Their properties and suppliers are summarized in Table I. Green fluorescent seed particles are used to study their retention at various flow rates. Nonfluorescent seed particles are used in subsequent NP trapping experiments.

D. Fluorescent nanoparticles

In the NP trapping studies, green fluorescent polystyrene NPs (see Table I), sold as 270-nm diameter, 1-wt % stock concentration, are used. The fluorescence excitation peak of the NPs is $\lambda_{ex} = 468$ nm and the emission peak is $\lambda_{em} = 508$ nm. The particles are analyzed by NP tracking analysis using a NanoSight LM10 (Malvern Analytical), which finds a mean diameter of 277 ± 50 nm and stock concentration of 5.8×10^{12} particles/ml.

E. Seed particle retention quantification

Seed particle washing experiments are performed on the AcouTrap system as detailed in Fig. 3, whereby fluorescent seed particles made of either polystyrene or silica (see Table I) are aspirated to form large clusters and washed at increasing flow rates until the cluster can no longer be retained and is washed away. To explore the dynamic range for retention of each seed particle, actuation voltages of 2, 4, 6, 8, and 10 V p.p. are tested, with three repeats for each condition.

Frequency tracking is turned off during steps 5 to 6 in Fig. 3 and the frequency is kept at the optimal value found after washing at 150 µl/min to avoid momentary losses in retention force during the frequency scans, which, at high flow rates, introduce variability to the results. The flow rate is ramped up (in steps defined in Fig. 3) every 5 s without stopping the flow. For each run, the critical flow rate Q_c is recorded, defined as the flow rate before the loss of the cluster occurs. From the Q_c values, we calculate a retention coefficient and the maximum retention force for each seed particle material.

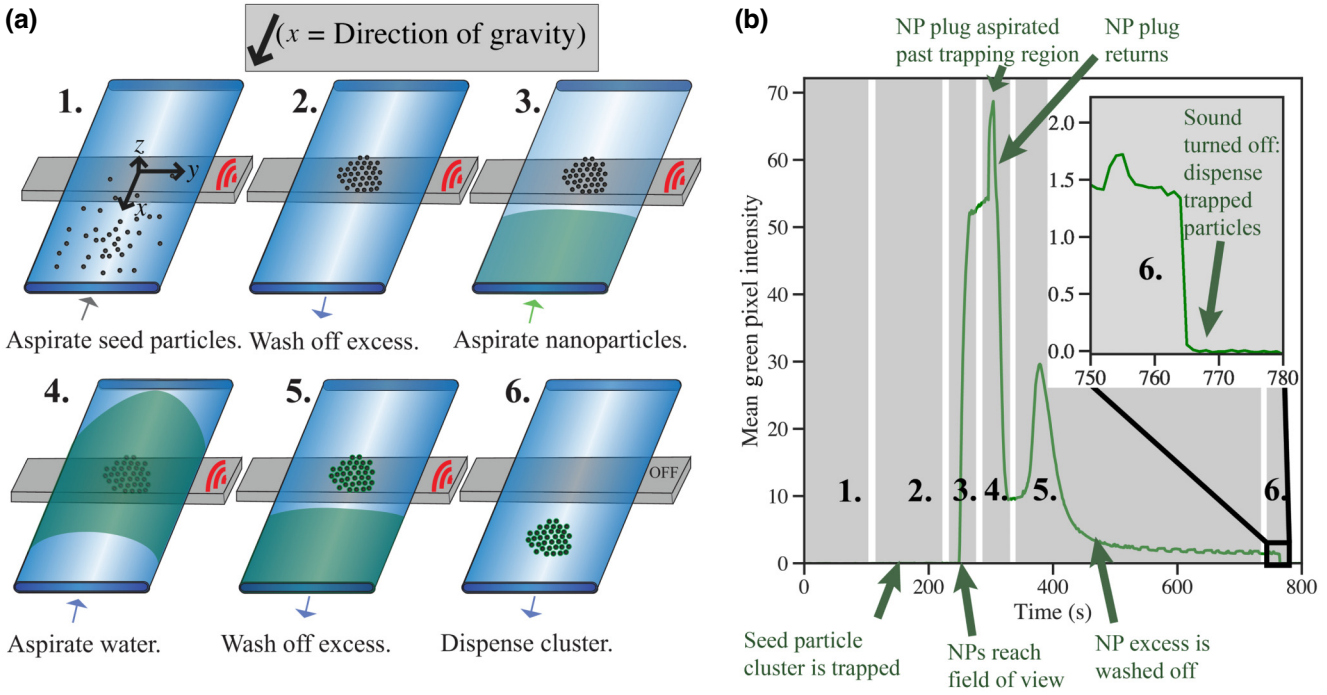

FIG. 4. (a) Schematic of acoustic trapping of fluorescent NPs (represented by green shading) into seed particle clusters (represented by grey circles). (b) A fluorescence-time profile resulting from a NP trapping experiment following the same steps. The steps are as follows: (1) the trap is turned on and 60 µl of freshly stirred seed particles are aspirated at 75 µl/min (or 100 µl/min in enhanced throughput studies); (2) excess seed particles are washed off dispensing 100 µl of water at 50 µl/min (or 200 µl of water at 100 µl/min in enhanced throughput studies); (3) 25 µl of the green fluorescent NPs are aspirated at 30 µl/min; (4) 25 µl of water is aspirated at 30 µl/min, so the plug of NPs passes the trapping region; (5) 200 µl of water is dispensed at 30 µl/min (or 200 µl/min in enhanced throughput studies) to bring the plug of NPs back past the trapping region, washing off excess NPs; (6) the ultrasound is switched off and then the cluster is dispensed with 200 µl water at 500 µl/min. Gravity acts in the positive x direction.

F. Nanoparticle trapping quantification

Acoustic trapping for several NP concentrations is performed with both silica and polystyrene seed particle clusters. In the protocol [described in detail in Fig. 4(a)], seed particle clusters are retained at 10 V p.p. (steps 1 and 2), after which the fluorescent NPs (polystyrene, 270-nm diameter) are aspirated as a plug and enriched into the seed particle cluster (steps 3–5). At step 6, the trapped NPs are released by turning the trap off before dispensing. The fluorescence-time profiles [Fig. 4(b)] are compared for different seed particle materials, NP concentrations, and wash flow rates.

The fluorescence intensity scales with the number of NPs in the field of view. The NP stock is diluted with MilliQ water (Merck KgaA, Darmstadt, Germany) to give the concentrations: (20, 10, and 2) $\times$ 10^{10} particles/ml. Figure 4(b) shows an example of a fluorescence profile during a trapping experiment; the exposure time of the camera is set for each NP concentration (1/125, 1/60, and 1/30 s, respectively, for decreasing concentration) to maximize the signal but avoid saturation to allow a clear comparison between the fluorescence-time profiles acquired with different seed particles at one NP concentration.

The first peak [between steps 3 and 4 in Fig. 4(b)] and second peak (early in step 5) indicate the plug of the NP sample passing the trapping region, first in the aspiration mode when water is aspirated (step 4), and then in the washing mode (step 5). The downward slope towards a plateau (after the peak in step 5) indicates washing off excess nontrapped NPs at a flow rate of 30 µl/min (step 5 in Fig. 4). At step 6, the ultrasound is turned off and the seed particle cluster is dispensed [inset Fig. 4(b)]; the fluorescence signal drop indicates the release of NPs that had been trapped. The trap off step, the fluorescence change observed when the cluster is released, is calculated from the green intensity before release (mean green pixel fluorescence in the 15 s before the sound is turned off) minus the baseline (mean fluorescence during the 10 s following dispensing).

A further set of experiments is performed to investigate enhanced throughput for NP trapping, where silica seed particles are used for NP trapping with a faster washing flow rate of 200 µl/min (as well as a 30-µl/min control).

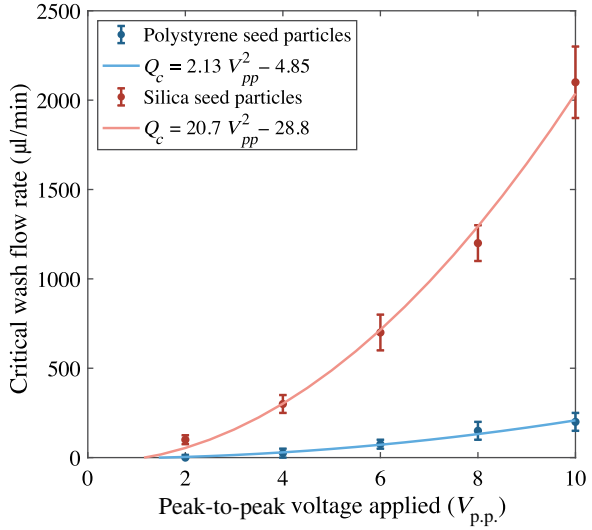

FIG. 5. Critical mean wash flow rates for silica (red) and polystyrene (blue) seed particles for 2–10 V p.p. (error bars indicate the estimated uncertainty due to the discrete flow rates measured). Corresponding best-fit lines defined by the equation $Q_c = c_r\ V_{pp}^2 + Q_0$ with the retention coefficient c_r for each seed particle.

In these enhanced throughput studies, silica seed particle aspiration and washing (steps 1 and 2 in Fig. 4) are performed at 100 µl/min to ensure a stable silica seed particle cluster before trapping fluorescent NPs at 10×10^{10} particles/ml (camera exposure time 1/60 s).

IV. RESULTS AND DISCUSSION

A. Seed particle retention flow rates

In the first experiments, clusters of seed particles are retained at different voltages and retained against increasing flow rates, see results in Fig. 5 and Table II. The critical flow rates reveal the equilibrium point between the drag force and retention force, i.e., the flow rate where clusters can just about be retained before being pulled out of the trap. At that flow rate, the fluid velocity at the cluster gives rise to a drag force F_d that is balanced with the retention force F_r, Eqs. (A1)–(A5). When actuated at 10 V p.p., polystyrene seed particles are lost after washing at a critical flow rate of $200 \pm 50\ \mu$l/min. In contrast, at 10 V p.p., silica seed particles are only lost after a critical flow rate of $2100 \pm 200\ \mu$l/min.

For both polystyrene and silica seed particles, the critical flow rates Q_c [corrected for gravity effects by Q_0, see Eqs. (A6)–(A12)] are proportional to the square of peak-to-peak voltage applied, $Q_c - Q_0 \propto V_{pp}^2$, as shown in the quadratic fit in Fig. 5. For each material this result corresponds with the theory that $Q_c - Q_0 \propto f_2\ V_{pp}^2$ [Eq. (A10)].

It would be expected that the retention coefficient c_r of a cluster of seed particles of some material would be proportional to the seed particle's dipole scattering coefficient f_2. In other words, the particle's propensity to be retained against flow depends on its density, as in Eqs. (1) and (2). Calculating the ratios between each coefficient for silica seed particles compared to polystyrene seed particles (from Table II) yields $f_2(\text{silica})/f_2(\text{polystyrene}) = 9.4$ and $c_r(\text{silica})/c_r(\text{polystyrene}) = 9.7$. These ratios correspond quite well given the errors of up to 10% in Q_c at high flow rates and the inhomogeneity of silica seed particle diameters (coefficient of variation for silica diameter is 20%, Table I).

Thus, we find good agreement between the acoustic retention force theory and flow rate experiments. It is also apparent that silica seed particles consistently outperform polystyrene seed particles, being retained against faster flow rates and at lower voltages. For example, Fig. 5 shows that it is possible to wash clusters at 100 µl/min for silica seed particles retained at 2–10 V p.p., but only for polystyrene seed particles retained at 8–10 V p.p. At these voltages, and corresponding pressure amplitudes, the retention forces on a polystyrene seed particle would be expected to be around 10 times lower than the retention forces on a silica seed particle of the same size. Here we find that the range of voltages and flow rates under which silica seed particles can be retained is much greater than for the polystyrene seed particles traditionally used.

TABLE II. Retention performance of seed particles.

Parameter	Polystyrene seed particles	Silica seed particles
f_2[a]	0.037	0.350
Q_c (µl/min)[b]	200 ± 50	2100 ± 200
F_d (nN)[c]	1.3 ± 0.3	14 ± 2
c_r (−)[d]	2.13	20.7
R^2 of fit	0.984	0.994

[a]Dipole scattering coefficient calculated from Eq. (2) using the suppliers' values for density (Table I).
[b]Maximum critical flow rate for a cluster held at 10 V p.p.
[c]Stokes drag force at Q_c for 10 V p.p. calculated for one particle via Eqs. (A4) and (A5).
[d]The retention coefficient of material c_r, such that $Q_c - Q_0 \propto V_{pp}^2$ can be written as $Q_c = c_r V_{pp}^2 + Q_0$.

B. Nanoparticle trapping with polystyrene and silica seed particles

During the second set of experiments, fluorescence intensity is used to quantify seed-particle-enabled NP enrichment via acoustic trapping during aspiration, washing, and dispensing (at 30 µl/min and 10 V p.p., as described in Fig. 4). Figure 10 (see Appendix C) presents images taken during each of the steps in the protocol

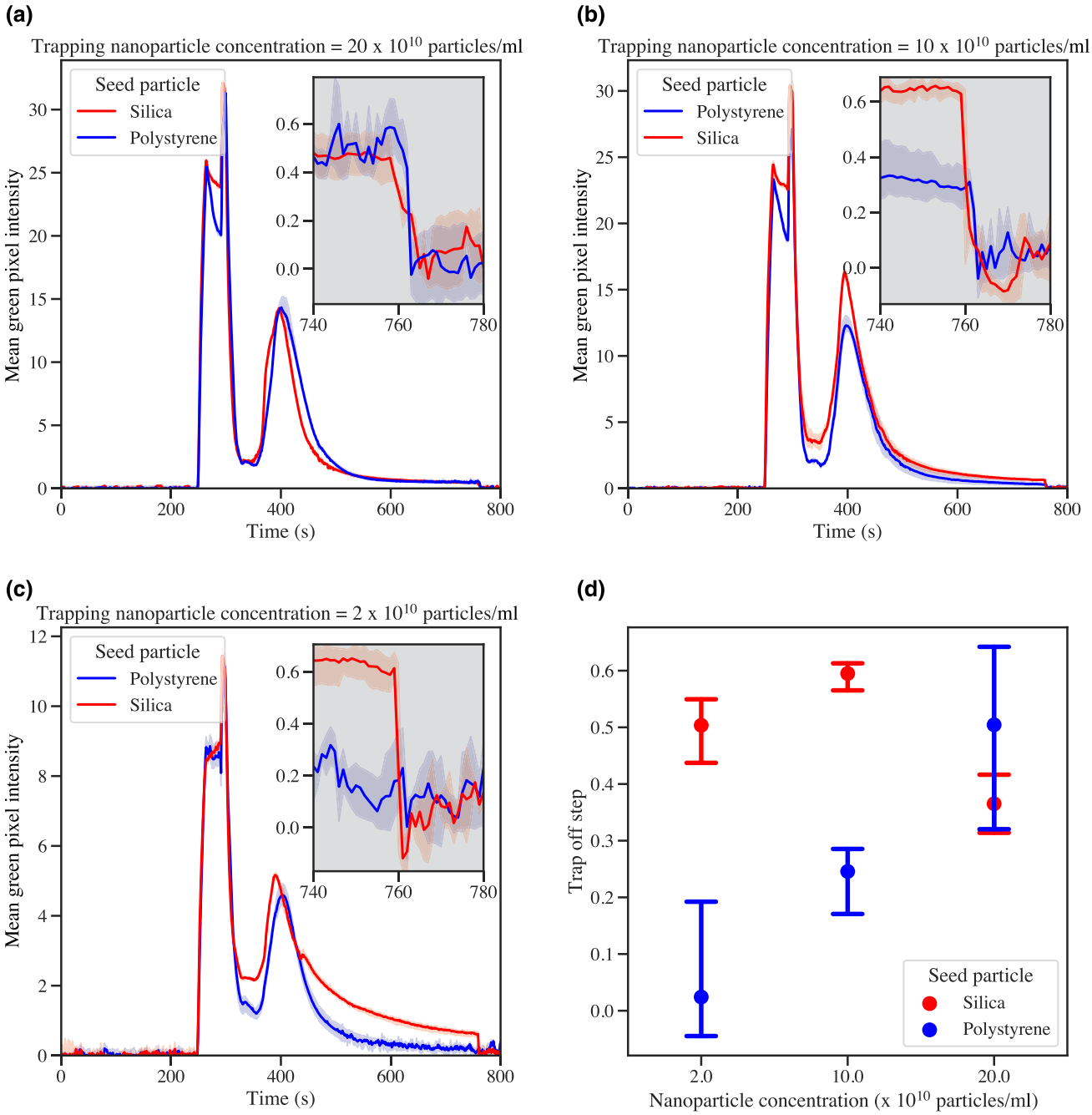

FIG. 6. (a)–(c) Graphs of fluorescence-time profiles [number of repeated experiments (N) = 2–4, error bars show the minimum and maximum for the respective experiments] for NP trapping quantification, with insets showing the trap off fluorescence change. The NPs aspirated had concentrations (and corresponding camera exposure times) of (a) 20×10^{10} particles/ml (at 1/125 s); (b) 10×10^{10} particles/ml (at 1/60 s); (c) 2×10^{10} particles/ml (at 1/30 s). (d) Shows that the trap off fluorescence change is negligible for trapping NPs at $<10^{11}$ particles/ml with polystyrene seed particles, but not silica seed particles (error bars show the minimum and maximum for each experiment).

(described in Fig. 4) and shows the enrichment of fluorescent NPs into the seed particle clusters. The fluorescence-time profiles of NP trapping under equal conditions are reasonably reproducible, see Figs. 6(a)–6(c), as the minimum and maximum are close to the mean.

The mean values of the trap off step (as defined in Sec. III F) are compared for silica and polystyrene seed particles in Fig. 6(d). For the highest NP concentration, 20×10^{10} particles/ml [Fig. 6(c)], silica performs similarly to polystyrene as a seed particle material; Fig. 6(d)

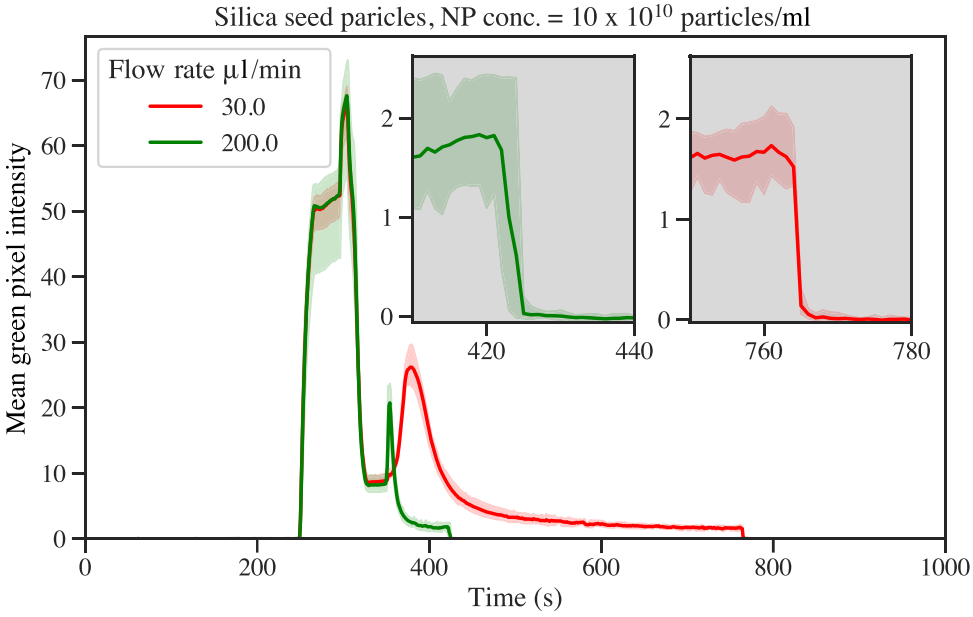

FIG. 7. Graph of fluorescence-time profile generated by trapping NPs with silica seed particles, six repeats. The NP trapping protocol (see Fig. 4) is followed, except in the washing step 5, where the flow rate is either 30 µl/min (red) or 200 µl/min (green). The trap off fluorescence change can be seen in the insets; the bounds of the slow wash (red) is well within the bounds of the fast wash (green) (error bars are minimum and maximum for each respective experiment, for $N = 6$).

indicates trap off step values for silica are within the trapping performance bounds (min-max) of polystyrene, albeit with a 30% lower mean. When the concentration of the NPs is halved to 10×10^{10} particles/ml [Fig. 6(b)], a difference in seed particle performance becomes apparent. Silica seed particles have a 40% higher mean trap off step than polystyrene seed particles. When the NP concentration is further decreased to only 2×10^{10} particles/ml [Fig. 6(a)], the difference in performance diverges further. Whereas polystyrene seed particles on average do not detectably trap NPs, silica appears to have an approximately 2000% higher mean trap off step, indicating that silica seed particles trap NPs with a greater efficiency than polystyrene NPs when handling dilute NP concentrations, below 10^{11} particles/ml.

The lower NP concentrations, $<10^{11}$ particles/ml for which silica outperforms polystyrene here, are close to the concentrations of extracellular vesicles $10^{9} - 10^{11}$ particles/ml found in biofluids such as cerebrospinal fluid, blood plasma, and urine [9,43,44]. Samples are also often diluted with phosphate-buffered saline to reduce the viscosity, thus trapping extracellular vesicles from samples around the order of 10^{10} particles/ml is desirable for many clinical applications.

C. Enhanced throughput nanoparticle trapping with silica seed particles

As the seed particle cluster washing experiments reveal (Table II), silica seed particles are easily retained at much higher flow rates than polystyrene, paving the way for increased sample throughput. Therefore, we investigate the effect of wash flow rate on NP trapping using silica seed particles without changing sample or wash volume.

Increasing the wash flow rate from 30 to 200 µl/min reduces the washing time from 7 to 1 min, and yet NPs are still trapped (see Fig. 7). Appendix C, Fig. 11 presents images taken during each of the steps in the protocol (described in Fig. 4) and shows the enrichment of fluorescent NPs into the silica seed particle clusters and the washing off.

The Fig. 7 insets show a 4% difference in mean trap off step when washing at 200 µl/min compared with the 30-µl/min washing. The trapping performance bounds (min-max) for the 200-µl/min flow rate wash encompasses the performance minimum and maximum values found for the slower flow rate wash. Thus, washing trapped NPs at 200 µl/min appears not to compromise trapping efficiency whilst enabling total processing time to be halved compared with a wash rate of 30 µl/min, providing silica seed particles are used to ensure the cluster is stable.

V. CONCLUSION

This work advances the acoustic trapping of NPs by challenging the status quo, which is currently to use polystyrene seed particles [9–12,19,31–35]. We demonstrate that silica seed particle clusters can trap NPs whilst washing at a flow rate of 200 µl/min, a flow rate at which the polystyrene seed particle clusters cannot be

easily retained due to polystyrene's low retention coefficient. Being able to wash at 200 µl/min with silica seed particles improves throughput for NP trapping, as the total sample processing time can be approximately halved from 13 to 7 min (cutting 6 min of wash time). Furthermore, dilute NPs, $\leq 10^{11}$ particles/ml, are trapped 40%–2000% more efficiently using silica instead of polystyrene seed particles. Silica seed particles therefore have advantages over polystyrene with higher throughput, increased trapping efficiency, and potentially better washing off of background proteins in biological samples. This makes them an attractive alternative for extracellular vesicle trapping in biofluids where high yield, high throughput, and low nonspecific isolation are desirable.

ACKNOWLEDGMENTS

This work was supported by the research Grants No. 2019-00795 and No. 2022-04041 from the Swedish Research Council and the travel grant scholarships from Stiftelsen för Mätcentrum Syd (awarded in 2022 and 2023).

The authors M.H. and T.B. have no conflicts of interest to declare that are relevant to the content of this article. T.L. is a founder and owns stock in AcouSort AB, and A.L. owns stock in AcouSort AB. AcouSort AB is a spin-off company from Lund University that manufactures and markets acoustofluidic technology. M.E. is an employee of and owns stock in AcouSort AB.

APPENDIX A: FORCES ON A SEED PARTICLE DURING ACOUSTIC TRAPPING

1. Stokes drag force

The critical flow velocity u_c (in m/s) has been defined as

$$u_c = \frac{\beta Q_c}{hw}, \tag{A1}$$

where β is 1.74, an aspect-ratio-dependent constant [39, 45]. Q_c is the critical flow rate (in µl/s), and h and w define the height (200 µm) and width (2000 µm) of the channel, respectively.

The drag force F_d acting on one particle of radius a in a fluid flow of velocity u is defined as

$$F_d = 6\pi\eta a\chi u, \tag{A2}$$

where χ is 1.06, derived from the wall-induced drag enhancement in the center of a parallel plate channel [39]. η is 0.89×10^{-3} Pa s, the viscosity of water at room temperature and pressure.

2. Retention force in equilibrium

The retention force acting on a seed particle in an acoustic trapping capillary can be determined by increasing the flow rate until the particle can no longer be retained. By using the drag force F_d at the critical flow rate for which the particles are retained in an acoustic trapping capillary mounted vertically, the gravitational force F_g, buoyancy force F_b, and finally the retention force F_r can be calculated.

$$F_g = \rho_p V g, \tag{A3}$$

$$F_b = \rho_f V g, \tag{A4}$$

$$F_r = F_d + F_g - F_b, \tag{A5}$$

where ρ_f is 997 kg m^{-3}, the density of water at room temperature and pressure, and ρ_p is the particle density. The gravitational constant g is 9.81 m/s. The volume of the particles is calculated as $V = 4/3\,\pi a^3$.

3. Critical flow rate—correcting for gravity

Approximately, for a single particle in equilibrium (i.e., the flow rate has been maximized to Q_c without overcoming the retention force),

$$F_d \approx F_r - Vg(\rho_p - \rho_f). \tag{A6}$$

Using Eqs. (A1)–(A5),

$$6\pi\eta a\chi u_c \approx V\frac{3 f_2 P_0^2}{8\,\omega^2\rho_f} k_x k_y^2 \sin(2k_x x) - Vg(\rho_p - \rho_f). \tag{A7}$$

If the particle size, position of the particles in the field, capillary geometry, and fluid are also constant,

$$u_c \propto f_2 P_0^2 - G_{\text{const}}(\rho_p), \tag{A8}$$

where G_{const} represents a constant independent of pressure and flow velocity, which, under the conditions stated, only depends on ρ_p and is given by

$$G_{\text{const}}(\rho_p) = \frac{3\chi g\omega^2\rho_f(\rho_p - \rho_f)}{8Vk_x k_y^2 \sin(2k_x x)}. \tag{A9}$$

By using Eq. (A1), $u_c \propto Q_c$, and by assuming the peak-to-peak voltage applied V_{pp} is proportional to the pressure amplitude, this gives

$$Q_c - Q_0(\rho_p) \propto f_2 V_{pp}^2, \tag{A10}$$

where the correction constant Q_0 is proportional to the difference between the particle density and fluid density,

$$Q_0(\rho_p) \propto \rho_p - \rho_f. \tag{A11}$$

When the flow rate is zero, some retention force (F_{r0}) is still required to retain the particles against gravity in

water,

$$F_{r0} = F_g - F_b = Vg(\rho_p - \rho_f). \tag{A12}$$

For a single seed particle with properties given in Table I, the zero-flow retention force from Eq. (A12) is $F_{r0}(\text{polystyrene}) = 0.3$ pN and $F_{r0}(\text{silica}) = 4.1$ pN. In a multiple-particle case, such as is the case for a trapped cluster of seed particles, the zero-flow retention force may be significantly larger. This has been observed for large seed particle clusters, which fall rapidly vertically (in the direction of gravity) when the sound is turned off. When holding a multiple-particle cluster against flow, the drag force on each particle can also be different than in the single-particle case.

APPENDIX B: THE IMPORTANCE OF RESONANCE FREQUENCY TRACKING

The AcouTrap system is set up to record both the resonance frequency and the temperature of the circuit board every 1 s. Upon turning on the piezoelectric transducer, as the transducer heats up, heat dissipation causes both the circuit board and water inside the capillary to increase in temperature. The former can be measured, and the latter can be inferred by the shift in resonance frequency from the change in speed of sound through water. Figure 8 shows the experimental results recorded with no applied fluid flow, indicating a 4-kHz frequency shift for each 1 °C temperature increase. Note that the fluid temperature would differ if instead there were an applied flow, replacing heated fluid with fluid at room temperature.

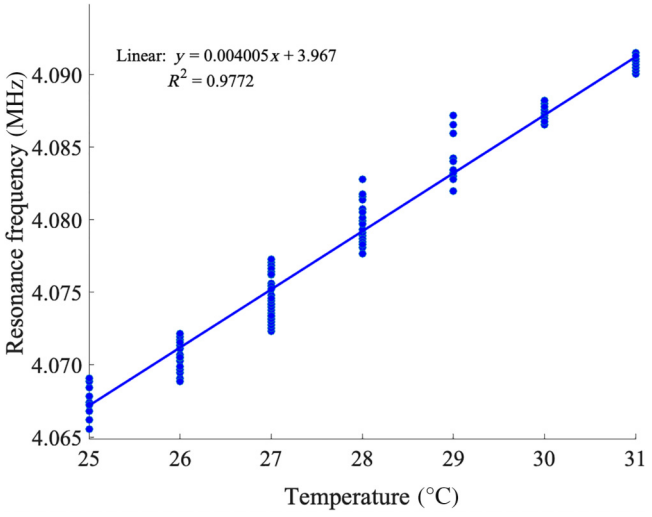

FIG. 8. Plot of experimental resonance frequency of the acoustic trapping capillary with increasing temperature. The temperature probe measured integer °C of the circuit board temperature and the resonance frequency of the water-filled capillary are measured simultaneously. This plot demonstrates the linear correlation between resonance frequency and temperature.

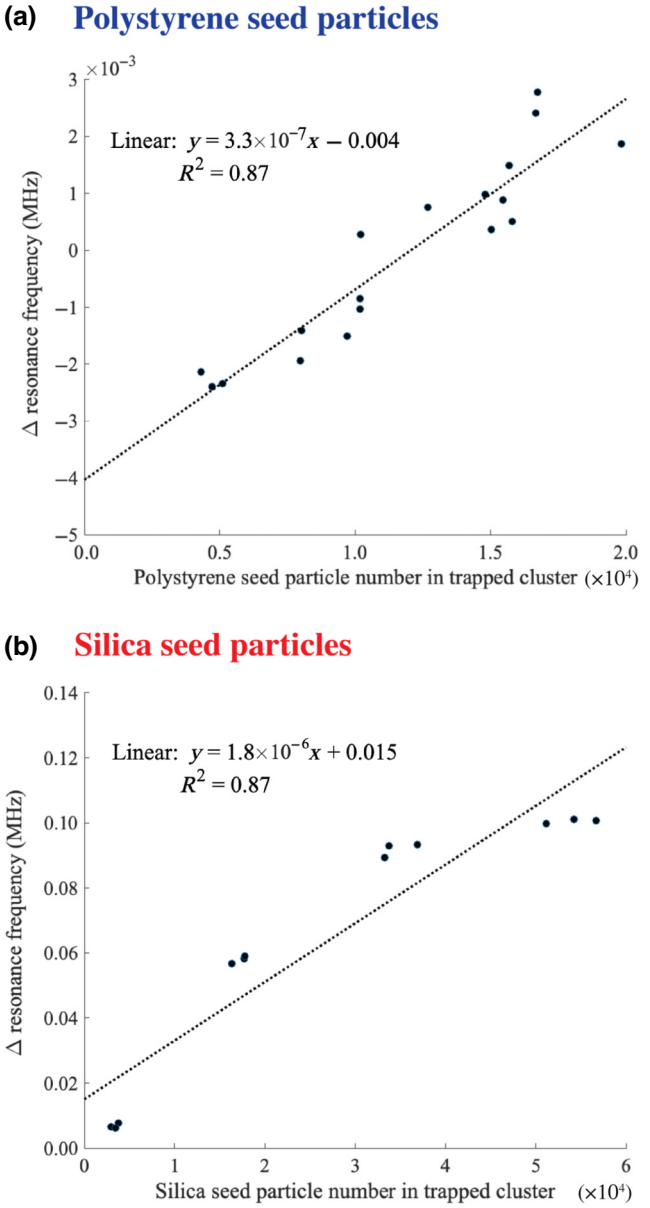

FIG. 9. The experimental measurement of the frequency shift (Δ resonance frequency compared to water-filled capillary with no seed particles) as increasing numbers of fluorescent 10-μm seed particles are trapped as a cluster for (a) polystyrene seed particles and (b) silica seed particles.

A further experiment, recording the resonance frequency, is performed with fluorescent seed particles present (silica and polystyrene). Before aspiration, the resonance frequency of the capillary is recorded once the frequency has stabilized. Seed particle clusters of varying sizes (from a small cluster up to the largest stable cluster) are trapped and washed to remove excess. The resonance frequency of the capillary, with the washed cluster, is recorded when the frequency is stable during a 60-s wait with zero flow, before turning the sound off and collecting the cluster by dispensing 150 μl of water into the 96-well

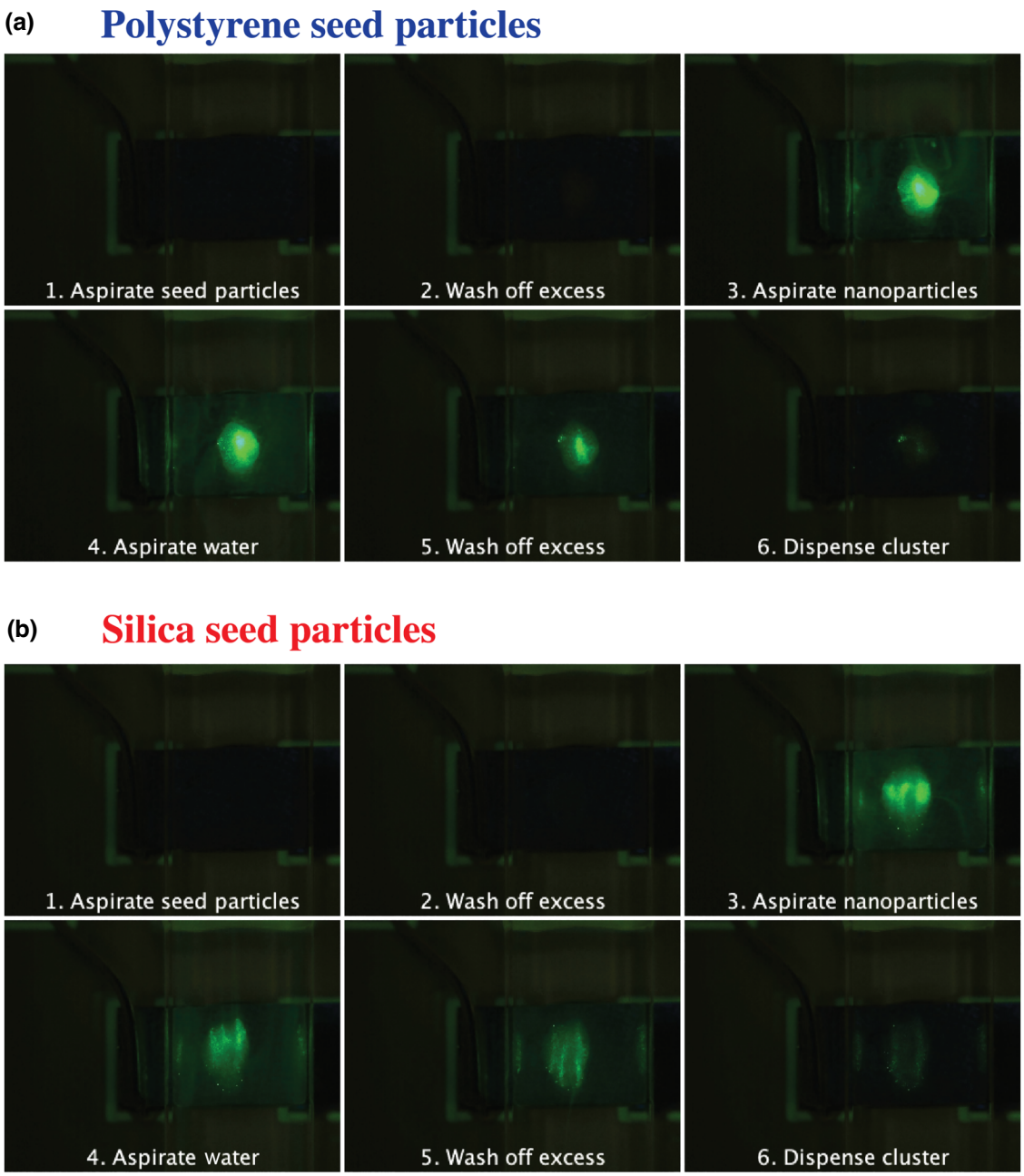

FIG. 10. Frames taken during each step of the NP trapping procedure (2×10^{10} particles/ml concentration exposure at 1/30 s) while using seed particles made of (a) silica and (b) polystyrene. The following steps are captured in each image: (1) an empty capillary; (2) seed particles (nonfluorescent); (3) NPs have reached the field of view and are enriched into the seed particle clusters, streaming pattern faintly visible; (4) plug of NPs has been aspirated past the trapping region; (5) the NP plug has returned and washing off of excess NPs is in progress; (6) washing is complete and the trapped NPs are ready to be dispensed.

plate. Each sample is added to a BD TruCount^{TM} absolute counting tube (lot number 48150, BD Biosciences), with which the particle count is measured by flow cytometry (BD FACSCanto II). Figure 9 shows resonance frequency shifts of up to 3 kHz for polystyrene clusters (around 0.3 Hz per bead) and up to 100 kHz for silica clusters (around 1.8 Hz per bead). This result for polystyrene beads is of the same order of magnitude as found previously [42], where the observed frequency shift was of the order of 1 Hz per nonfluorescent 12-μm polystyrene bead.

APPENDIX C: TIME-SERIES IMAGES FROM NANOPARTICLE TRAPPING

Figures 10 and 11 show image sequences from NP trapping experiments. These qualitatively show how NPs

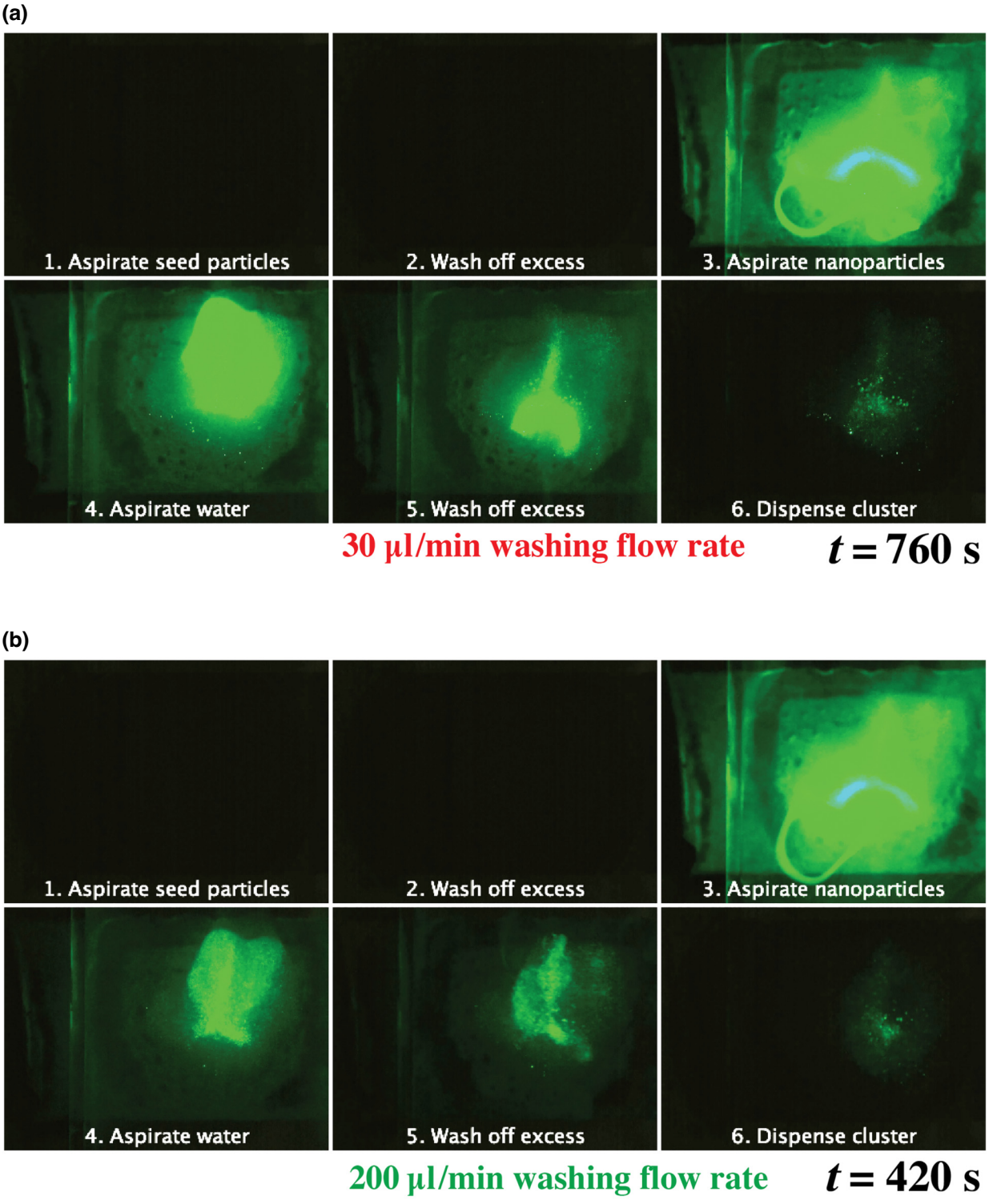

FIG. 11. Frames taken during each step of the NP trapping procedure (10×10^{10} particles/ml) with silica seed particles and washing flow rate (a) 30 µl/min and (b) 200 µl/min. These images have a higher magnification than previous ones, and grayscale maximum has been reduced from 255 to 100 to increase brightness. The following can be seen in each image: (1) an empty capillary; (2) silica seed particles (nonfluorescent); (3) NPs have reached the field of view and are enriched into the silica seed particle clusters, acoustic streaming pattern faintly visible; (4) plug of NPs has been aspirated past the trapping region; (5) the NP plug has returned and excess washing off of NPs is in progress; (6) washing is complete and the trapped NPs are ready to be dispensed.

are enriched and then excess is washed off during the trapping procedure. The images correspond to the annotations given in the schematic fluorescence graph in Fig. 4.

[1] G. Raposo, H. W. Nijman, W. Stoorvogel, R. Leijendekker, C. Harding, C. Melief, and H. Geuze, B lymphocytes secrete antigen-presenting vesicles, J. Exp. Med. **183**, 1161 (1996).

[2] R. Kalluri and V. S. LeBleu, The biology, function, and biomedical applications of exosomes, Science **367**, eaau6977 (2020).

[3] A. V. Vlassov, S. Magdaleno, R. Setterquist, and R. Conrad, Exosomes: Current knowledge of their composition, biological functions, and diagnostic and therapeutic potentials, Biochim. Biophys. Acta **1820**, 940 (2012).

[4] M. Havers, A. Broman, A. Lenshof, and T. Laurell, Advancement and obstacles in microfluidics-based isolation of extracellular vesicles, Anal. Bioanal. Chem. **415**, 1265 (2022).

[5] C. Théry, *et al.*, Minimal information for studies of extracellular vesicles 2018 (MISEV2018): A position statement of the international society for extracellular vesicles and update of the MISEV2014 guidelines, J. Extracell. Vesicles **7**, 1535750 (2018).

[6] B. J. Tauro, D. W. Greening, R. A. Mathias, H. Ji, S. Mathivanan, A. M. Scott, and R. J. Simpson, Comparison of ultracentrifugation, density gradient separation, and immunoaffinity capture methods for isolating human colon cancer cell line LIM1863-derived exosomes, Methods **56**, 293 (2012).

[7] A. Gámez-Valero, M. Monguió-Tortajada, L. Carreras-Planella, M. Franquesa, K. Beyer, and F. E. Borràs, Size-exclusion chromatography-based isolation minimally alters extracellular vesicles' characteristics compared to precipitating agents, Sci. Rep. **6**, 33641 (2016).

[8] B. Hammarström, T. Laurell, and J. Nilsson, Seed particle-enabled acoustic trapping of bacteria and nanoparticles in continuous flow systems, Lab Chip **12**, 4296 (2012).

[9] A. Ku, H. C. Lim, M. Evander, H. Lilja, T. Laurell, S. Scheding, and Y. Ceder, Acoustic enrichment of extracellular vesicles from biological fluids, Anal. Chem. **90**, 8011 (2018).

[10] M. Evander, O. Gidlöf, B. Olde, D. Erlinge, and T. Laurell, Non-contact acoustic capture of microparticles from small plasma volumes, Lab Chip **15**, 2588 (2015).

[11] A. Broman, A. Lenshof, M. Evander, L. Happonen, A. Ku, J. Malmström, and T. Laurell, Multinodal acoustic trapping enables high capacity and high throughput enrichment of extracellular vesicles and microparticles in miRNA and MS proteomics studies, Anal. Chem. **93**, 3929 (2021).

[12] D. Paget, A. Checa, B. Zährer, R. Heilig, M. Shanmuganathan, R. Dhaliwal, E. Johnson, M. M. Jørgensen, R. Bæk, Oxford Acute Myocardial Infarction Study (OxAMI), C. E. Wheelock, K. M. Channon, R. Fischer, D. C. Anthony, R. P. Choudhury, and N. Akbar, Comparative and integrated analysis of plasma extracellular vesicle isolation methods in healthy volunteers and patients following myocardial infarction, J. Extracell. Biol. **1**, e66 (2022).

[13] M. Wiklund and H. M. Hertz, Ultrasonic enhancement of bead-based bioaffinity assays, Lab Chip **6**, 1279 (2006).

[14] M. Evander, L. Johansson, T. Lilliehorn, J. Piskur, M. Lindvall, S. Johansson, M. Almqvist, T. Laurell, and J. Nilsson, Noninvasive acoustic cell trapping in a microfluidic perfusion system for online bioassays, Anal. Chem. **79**, 2984 (2007).

[15] M. Settnes and H. Bruus, Forces acting on a small particle in an acoustical field in a viscous fluid, Phys. Rev. E: Stat., Nonlinear, Soft Matter Phys. **85**, 016327 (2012).

[16] L. P. Gor'kov, On the forces acting on a small particle in an acoustical field in an ideal fluid, Sov. Phys. **6**, 773 (1962).

[17] K. Yosioka and Y. Kawasima, Acoustic radiation pressure on a compressible sphere, Acta Acustica united with Acustica **5**, 167 (1955).

[18] A. Fornell, T. Baasch, C. Johannesson, J. Nilsson, and M. Tenje, Binary acoustic trapping in a glass capillary, J. Phys. D: Appl. Phys. **54**, 355401 (2021).

[19] A. Ku, J. Fredsøe, K. D. Sørensen, M. Borre, M. Evander, T. Laurell, H. Lilja, and Y. Ceder, High-throughput and automated acoustic trapping of extracellular vesicles to identify microRNAs with diagnostic potential for prostate cancer, Front. Oncol. **11**, 631021 (2021).

[20] S. Gupta and D. L. Feke, Acoustically driven collection of suspended particles within porous media, Ultrasonics **35**, 131 (1997).

[21] G. T. Silva and H. Bruus, Acoustic interaction forces between small particles in an ideal fluid, Phys. Rev. E: Stat., Nonlinear, Soft Matter Phys. **90**, 063007 (2014).

[22] T. Baasch, W. Qiu, and T. Laurell, Gap distance between pearl chains in acoustic manipulation, Phys. Rev. Appl. **18**, 014021 (2022).

[23] T. Baasch, I. Leibacher, and J. Dual, Multibody dynamics in acoustophoresis, J. Acoust. Soc. Am. **141**, 1664 (2017).

[24] A. R. Mohapatra, S. Sepehrirahnama, and K. M. Lim, Experimental measurement of interparticle acoustic radiation force in the Rayleigh limit, Phys. Rev. E **97**, 053105 (2018).

[25] D. Saeidi, M. Saghafian, S. H. Javanmard, and M. Wiklund, A quantitative study of the secondary acoustic radiation force on biological cells during acoustophoresis, Micromachines **11**, 152 (2020).

[26] B. G. Winckelmann and H. Bruus, Acoustic radiation force on a spherical thermoviscous particle in a thermoviscous fluid including scattering and microstreaming, Phys. Rev. E **107**, 065103 (2023).

[27] A. Pavlic, L. Ermanni, and J. Dual, Interparticle attraction along the direction of the pressure gradient in an acoustic standing wave, Phys. Rev. E **105**, L053101 (2022).

[28] S. Sepehrirahnama, F. S. Chau, and K. M. Lim, Effects of viscosity and acoustic streaming on the interparticle radiation force between rigid spheres in a standing wave, Phys. Rev. E **93**, 023307 (2016).

[29] S. Sepehrirhnama and K. M. Lim, Generalized potential theory for close-range acoustic interactions in the Rayleigh limit, Phys. Rev. E **102**, 043307 (2020).

[30] J. H. Joergensen and H. Bruus, Theory of pressure acoustics with thermoviscous boundary layers and streaming in elastic cavities, J. Acoust. Soc. Am. **149**, 3599 (2021).

[31] A. Ku, N. Ravi, M. Yang, M. Evander, T. Laurell, H. Lilja, and Y. Ceder, A urinary extracellular vesicle microRNA biomarker discovery pipeline; From automated extracellular vesicle enrichment by acoustic trapping to microRNA sequencing, PLOS ONE **14**, e0224604 (2019).

[32] O. Gidlöf, M. Evander, M. Rezeli, G. Marko-Varga, T. Laurell, and D. Erlinge, Proteomic profiling of extracellular vesicles reveals additional diagnostic biomarkers for myocardial infarction compared to plasma alone, Sci. Rep. **9**, 8991 (2019).

[33] Melinda Rezeli, Olof Gidlöf, Mikael Evander, Paulina Bryl-Górecka, Ramasri Sathanoori, Patrik Gilje, Krzysztof Pawłowski, Péter Horvatovich, David Erlinge, György Marko-Varga, and Thomas Laurell, Comparative proteomic analysis of extracellular vesicles isolated by acoustic trapping or differential centrifugation, Anal. Chem. **88**, 8577 (2016).

[34] P. Bryl-Górecka, R. Sathanoori, L. Arevström, R. Landberg, C. Bergh, M. Evander, B. Olde, T. Laurell, O. Fröbert, and D. Erlinge, Bilberry supplementation after myocardial infarction decreases microvesicles in blood and affects endothelial vesiculation, Mol. Nutr. Food Res. **64**, 2000108 (2020).

[35] F. Palm, A. Broman, G. Marcoux, J. W. Semple, T. L. Laurell, J. Malmström, and O. Shannon, Phenotypic characterization of acoustically enriched extracellular vesicles from pathogen-activated platelets, J. Innate Immun. **15**, 599 (2023).

[36] R. Habibi and A. Neild, Sound wave activated nano-sieve (SWANS) for enrichment of nanoparticles, Lab Chip **19**, 3032 (2019).

[37] R. Habibi, V. He, S. Ghavamian, A. De Marco, T. H. Lee, M. I. Aguilar, D. Zhu, R. Lim, and A. Neild, Exosome trapping and enrichment using a sound wave activated nano-sieve (SWANS), Lab Chip **20**, 3633 (2020).

[38] B. Hammarström, B. Nilson, T. Laurell, J. Nilsson, and S. Ekström, Acoustic trapping for bacteria identification in positive blood cultures with MALDI-TOF MS, Anal. Chem. **86**, 10560 (2014).

[39] M. W. H. Ley and H. Bruus, Three-dimensional numerical modeling of acoustic trapping in glass capillaries, Phys. Rev. Appl. **8**, 024020 (2017).

[40] W. Qiu, J. T. Karlsen, H. Bruus, and P. Augustsson, Experimental characterization of acoustic streaming in gradients of density and compressibility, Phys. Rev. Appl. **11**, 024018 (2019).

[41] K. Han, J. Suh, and G. Bahl, Optomechanical non-contact measurement of microparticle compressibility in liquids, Opt. Express **26**, 31908 (2018).

[42] B. Hammarström, M. Evander, J. Wahlström, and J. Nilsson, Frequency tracking in acoustic trapping for improved performance stability and system surveillance, Lab Chip **14**, 1005 (2014).

[43] Alexander G. Thompson, Elizabeth Gray, Imre Mager, Roman Fischer, Marie-Laëtitia Thézénas, Philip D. Charles, Kevin Talbot, Samir El Andaloussi, Benedikt M. Kessler, Matthew Wood, and Martin R. Turner, UFLC-derived CSF extracellular vesicle origin and proteome, Proteomics **18**, 1800257 (2018).

[44] K. B. Johnsen, J. M. Gudbergsson, T. L. Andresen, and J. B. Simonsen, What is the blood concentration of extracellular vesicles? Implications for the use of extracellular vesicles as blood-borne biomarkers of cancer, Biochim. Biophys. Acta Rev. Cancer **1871**, 109 (2019).

[45] H. Bruus, *Theoretical Microfluidics* (Oxford University Press, Oxford, 2007), Vol. 18.